Journal for ImmunoTherapy of Cancer

Liver-directed AAV-IL-10 therapy enhances CD8$^+$ T cell-mediated immunity against hepatocellular carcinoma

Chia-I Lin,[1] Yi-Wei Chiu,[1] Meng-Syuan Yen,[1] Yu-Wen Wang,[1] Ying-Hsuan Wu,[1] Ya-Hui Chuang [1,2]

To cite: Lin C-I, Chiu Y-W, Yen M-S, *et al*. Liver-directed AAV-IL-10 therapy enhances CD8$^+$ T cell-mediated immunity against hepatocellular carcinoma. *Journal for ImmunoTherapy of Cancer* 2026;**14**:e012460. doi:10.1136/jitc-2025-012460

► Additional supplemental material is published online only. To view, please visit the journal online (https://doi.org/10.1136/jitc-2025-012460).

Accepted 02 March 2026

[1]Department of Clinical Laboratory Sciences and Medical Biotechnology, National Taiwan University, Taipei, Taiwan
[2]Department of Laboratory Medicine, National Taiwan University Hospital, Taipei, Taiwan

Correspondence to
Dr Ya-Hui Chuang;
yahuichuang@ntu.edu.tw

ABSTRACT

Background The liver's inherently immunosuppressive microenvironment presents a major barrier to effective immunotherapy for hepatocellular carcinoma (HCC). Although interleukin-10 (IL-10) has demonstrated antitumor activity in several cancer models, its therapeutic potential in HCC remains unclear. Here, we investigated whether liver-directed delivery of IL-10 using an adeno-associated virus vector (AAV-IL-10) could enhance antitumor immunity in HCC.

Methods Syngeneic orthotopic and intrahepatic metastatic HCC mouse models were used to evaluate the effects of liver-directed AAV-IL-10 therapy. Tumor burden, immune cell infiltration, and functional activation were assessed by flow cytometry and related analyses.

Results Liver-directed AAV-IL-10 treatment significantly reduced intrahepatic tumor burden and promoted robust infiltration of CD8$^+$ T cells into the tumor microenvironment. AAV-IL-10 enhanced the functional activation of natural killer cells and CD8$^+$ T cells, as reflected by increased expression of effector cytokines and cytotoxic molecules. Notably, AAV-IL-10 augmented the effector capacity of terminally exhausted CD8$^+$ tumor-infiltrating lymphocytes and expanded a population of CD8$^+$ T cells with a tissue-resident memory (Trm)-like phenotype. These Trm-like CD8$^+$ T cells were liver-resident and persisted after tumor clearance. Importantly, the antitumor effects of AAV-IL-10 were confined to the liver and did not affect the growth of distant subcutaneous tumors.

Conclusions Liver-directed AAV-IL-10 delivery overcomes local immunosuppression and enhances CD8$^+$ T cell-mediated antitumor immunity in murine HCC models. These findings support targeted IL-10 delivery as a promising strategy to improve immunotherapy outcomes in liver cancer.

WHAT IS ALREADY KNOWN ON THIS TOPIC

⇒ Hepatocellular carcinoma (HCC) thrives within the liver's profoundly immunosuppressive environment, limiting the success of immunotherapy. While interleukin (IL)-10 has been shown to exert antitumor effects in certain cancers, its role in modulating liver-specific immunity in HCC remained unclear.

WHAT THIS STUDY ADDS

⇒ We demonstrate that liver-directed delivery of IL-10 using an adeno-associated virus vector not only reduces tumor burden but also reshapes the liver immune landscape by enhancing CD8$^+$ T-cell effector function and promoting the development of long-lived, tissue-resident memory-like CD8$^+$ T cells.

HOW THIS STUDY MIGHT AFFECT RESEARCH, PRACTICE OR POLICY

⇒ This study identifies liver-directed IL-10 therapy as a novel strategy to break liver immune tolerance, paving the way for new approaches to improve immunotherapy efficacy in HCC and potentially other liver-associated cancers.

BACKGROUND

Hepatocellular carcinoma (HCC), which makes up about 90% of primary liver cancers, typically arises in a chronically inflamed and fibrotic liver, often linked to hepatitis B or C infections, toxins such as aflatoxins or alcohol, or metabolic disorders like non-alcoholic fatty liver disease and non-alcoholic steatohepatitis.[1] Despite advancements in systemic therapies, including targeted agents and immune checkpoint inhibitors, HCC remains difficult to treat effectively, largely due to the liver's unique immunological landscape. As an organ constantly exposed to gut-derived antigens and microbial products via the portal circulation, the liver has evolved a tolerogenic immune environment to prevent excessive inflammation. While this immunosuppressive milieu serves a protective physiological role, it becomes a major obstacle in HCC by dampening antitumor immune responses and facilitating tumor progression.[2 3]

CD8$^+$ T cells, particularly those specific to tumor antigens, are the key subset of tumor-infiltrating lymphocytes (TILs) responsible for antitumor activity.[3–5] They eliminate

tumor cells by inducing apoptosis through the release of perforin and granzyme B or by engaging the Fas/Fas ligand pathway. Additionally, $CD8^+$ T cells secrete cytokines like interferon-gamma (IFN-γ) and tumor necrosis factor-alpha (TNF-α) to enhance their antitumor effects.[6] In murine HCC models, the absence of $CD8^+$ T cells accelerates tumor growth,[7] while in human HCC, a high presence of tumor antigen-specific $CD8^+$ TILs correlates with improved survival and reduced disease progression.[8] However, most $CD8^+$ T cells in human HCC are dysfunctional.[9–11]

Interleukin-10 (IL-10) is widely recognized for its potent anti-inflammatory and immunosuppressive functions. It downregulates the expression of major histocompatibility complex class II and costimulatory molecules and suppresses the production of pro-inflammatory cytokines in antigen-presenting cells such as macrophages and dendritic cells. IL-10 can also directly inhibit $CD4^+$ T-cell activation while promoting the maintenance, proliferation, and suppressive function of regulatory T cells.[12 13] However, IL-10 also has well-established immune-stimulatory effects, particularly on $CD8^+$ T cells. In several tumor models, therapeutic administration of IL-10 or localized IL-10 expression has been shown to enhance $CD8^+$ T-cell proliferation, effector function, and cytotoxicity, resulting in tumor regression.[14–18] Clinical studies similarly demonstrate that recombinant IL-10 can augment $CD8^+$ T cell-mediated antitumor immunity in patients, without causing notable systemic toxicity.[19 20] Moreover, in our previous study using a mouse model of primary biliary cholangitis, liver-directed delivery of IL-10 via adeno-associated virus (AAV) activated intrahepatic $CD8^+$ T cells and induced proinflammatory immune responses within the liver.[21] These findings highlight IL-10 as a context-dependent cytokine capable of both suppressing and promoting immune responses. However, how IL-10 functions within the immunosuppressive tumor microenvironment of the liver, where immune activation is tightly regulated, remains unclear.

Recombinant IL-10 protein exhibits a short half-life, necessitating frequent administration to maintain therapeutic levels.[22] For liver cancer, achieving sustained and localized expression of IL-10 within the liver is critical for therapeutic efficacy. This requires an efficient gene delivery system with precise targeting capabilities. Recombinant AAV vectors are highly suitable for in vivo gene transfer due to their replication-deficient nature, ability to transduce a broad range of cell types—including non-dividing cells—capacity for long-term expression, and low immunogenicity compared with earlier-generation adenoviral vectors.[23] Furthermore, the liver is one of the principal sites where AAV-based gene therapy is being applied successfully in humans.[24]

In this study, we investigated whether liver-directed delivery of IL-10 using an adeno-associated virus vector (AAV-IL-10) could enhance antitumor immunity and suppress tumor progression in syngeneic mouse models of HCC, including orthotopic primary and intrahepatic metastatic tumor models. Both models rapidly and reproducibly establish intrahepatic tumors and closely recapitulate the immunosuppressive hepatic tumor microenvironment characteristic of human HCC.[25] By localizing IL-10 expression primarily to the liver, AAV-IL-10 treatment effectively suppressed liver tumor growth. This strategy enhanced $CD8^+$ T-cell infiltration and activation within the tumor microenvironment, resulting in a strong antitumor immune response. Notably, we also observed an expansion of a distinct population of $CD8^+$ T cells with a tissue-resident memory (Trm) phenotype in tumors of AAV-IL-10-treated mice. These findings suggest that liver-directed IL-10 therapy represents a promising advancement in immunotherapy for HCC.

METHODS

Preparation of AAV-IL-10 and AAV-mock

AAV-IL-10 was generated by cloning the mouse IL-10 coding sequence, flanked by restriction enzyme sites, into the multiple cloning site of the pAAV-IRES-GFP vector (Cell Biolabs). The resulting plasmid, pAAV-IL-10-IRES-GFP, was co-transfected with pAAV-DJ and pAAV-Helper plasmids at a 1:1:1 ratio into HEK293 cells. Following transfection, viral particles were harvested from infected cells through three freeze-thaw cycles and subsequently purified by CsCl density-gradient centrifugation. AAV-mock, which lacks the IL-10 transgene, was prepared using the same procedure. Viral titers were determined by real-time PCR (quantitative PCR (qPCR)) targeting the green fluorescent protein (GFP) sequence within the viral genome. Viral DNA was extracted using the QIAamp DNA Blood Mini Kit (QIAGEN), and qPCR was performed using the forward primer ACGTCTATATCATGGCCG and reverse primer TGTGATCGCGCTTCTC.

HCC tumor cell line

The Hep55.1c cell line, derived from DENA-induced HCC in C57BL/6 mice, was obtained from Cell Line Service (Emmelheim). To generate stable OVA-expressing clones, the parental Hep55.1c cells were transfected with a lentiviral vector encoding the ovalbumin (OVA) gene. Single-cell clones were isolated in 96-well plates by serial dilution, and OVA expression levels in each clone were evaluated by real-time quantitative PCR (RT-qPCR) and western blotting. Clones exhibiting the lowest levels of OVA expression were selected for subsequent experiments and designated as Hep55.1c-OVA.

Tumor mouse models

C57BL/6 male mice were purchased from the National Laboratory Animal Center, Taiwan, and maintained in the Animal Center of the College of Medicine, National Taiwan University. For the orthotopic HCC mouse model, 2×10^6 Hep55.1c or Hep55.1c-OVA cells suspended in 20 µL of 20% Matrigel (Corning, #354234) were injected into the left lateral lobe of the liver in anesthetized 7–9 weeks old mice. For the intrahepatic metastasis

model, 1×10^6 Hep55.1c-OVA in 100 µL normal saline was injected into the spleen, and the spleen was excised 5 min later. For the subcutaneous model, 2×10^6 Hep55.1c cells in 50 µL of 50% Matrigel were injected subcutaneously into the right leg of anesthetized mice. Tenoxicam (1 mg/kg) was administered 24, 48, and 72 hours after surgery to manage postoperative inflammation. Hep55.1c tumor cells were intrahepatically inoculated into C57BL/6 mice on day 0. 5 days after tumor inoculation, mice received an intravenous injection of either AAV-IL-10 or AAV-mock (3×10^{10} genome copies/mouse). In the $CD8^+$ T-cell depletion experiment, mice received anti-CD8 antibodies (Bio X Cell, clone 2.43) or isotype control antibodies (Bio X Cell, clone LTF-2) starting 1 day before AAV administration and continuing until the end of the experiment (100 µg/mouse, two times a week). All experimental procedures were approved by the Institutional Animal Care and Use Committee of the National Taiwan University College of Medicine (No: 20210370; 20240381).

Serum IL-10 ELISA

Serum IL-10 levels were measured using a commercial ELISA kit (Duoset; R&D Systems). Blood was collected via retro-orbital bleeding using non-heparinized microhematocrit capillaries (Assistent) into 1.5 mL microcentrifuge tubes, left at room temperature for at least 1 hour to allow complete clotting, and then centrifuged at 5,500 rpm for 5 min to separate the serum, which was carefully collected and stored at −20°C until analysis.

Tumor-infiltrating leukocytes isolation

Tumors were dissected from mice, weighed, mechanically minced, and digested by stirring at 80 rpm in Roswell Park Memorial Institute (RPMI)-1640 medium containing collagenase type IV (25,000 U/mL, Gibco/Thermo Fisher Scientific), hyaluronidase (30,000 U/mL, Sigma-Aldrich), and DNase (10,000 U/mL, Sigma-Aldrich) at 37°C for 30 min. Tumor-infiltrating leukocytes were then isolated by density gradient centrifugation using Percoll (GE/Cytiva) and resuspended in 0.2% bovine serum albumin (BSA) in phosphate buffered saline (PBS). Red blood cell lysis was performed using ACK lysing buffer.

Flow cytometry analysis

Subsets and functional assays of TILs were analyzed using flow cytometry. For surface marker staining, TILs (1×10^6 cells per tube) were first incubated with Zombie dye (BioLegend) at room temperature for 15 min in the dark to label dead cells, followed by washing with 0.2% BSA in PBS. After centrifugation, cells were blocked with FcγR blocker in 0.2% BSA/PBS at 4°C for 10 min, then stained with fluorophore-conjugated monoclonal antibodies in 0.2% BSA/PBS at 4°C for 30 min in the dark, OVA-specific $CD8^+$ T cells were labeled by Allophycocyanin (APC) or Phycoerythrin (PE)-conjugated tetramer of the H-$2K^b$-restricted $OVA_{257–264}$ (SIINFEKL) peptide, which were obtained through the NIH Tetramer Core Facility (Emory University). Following another wash, cells were fixed in 1% paraformaldehyde. For intracellular cytokine staining, TILs were stimulated with 50 ng/mL phorbol-12-myristate-13-acetate (PMA; Cayman) and 1 µg/mL ionomycin (Abcam) in the presence of brefeldin A and monensin for 2 hours. After stimulation, cells were stained for surface markers, fixed, permeabilized using the Fixation/Permeabilization Solution Kit (BD Biosciences), and stained with antibodies targeting intracellular cytokines at 4°C for 30 min in the dark. For detection of Ki67 and TCF-1, cells were stained for surface markers, permeabilized using the True-Nuclear Transcription Factor Buffer Set (BioLegend) according to the manufacturer's instructions, and stained with anti-Ki67 or anti-TCF-1 monoclonal antibodies. Stained cells were analyzed using either a 4-laser Attune NxT flow cytometer (Thermo Fisher Scientific) or a 5-laser Aurora flow cytometer (Cytek Biosciences) with technical support from the Flow Cytometric Analyzing and Sorting Core Facility at National Taiwan University Hospital. Data were processed using FlowJo software (V.10; TreeStar). The Zombie Fixable Viability Kit (BioLegend) was used in all experiments to exclude dead cells from analysis. Fluorescence minus one and isotype controls were included to define gating strategies. A complete list of fluorochrome-conjugated monoclonal antibodies used is provided in table 1.

FTY720 treatment

7–9 weeks old male C57BL/6 mice were treated with intraperitoneal injections of FTY720 (Fingolimod; MCE, HY-12005, 0.025 mg in 100 µL normal saline) beginning 1 day prior to Hep55.1c-OVA cell inoculation. FTY720 was administered three times per week. On day 14, TILs, celiac lymph nodes (LNs), and portal LNs—the primary draining LNs of the liver[26]—were collected to assess OVA-specific $CD8^+$ T cells. Additionally, peripheral blood was collected using EDTA-coated tubes for blood cell isolation. Briefly, 100 µL of whole blood was incubated with 1 mL of RBC lysis buffer (BioLegend) at room temperature for 15 min, followed by centrifugation at 5,500 rpm for 2 min. The supernatant was discarded, and the remaining cell pellet was resuspended in 1 mL of 0.2% BSA in PBS for subsequent cell counting.

Immunohistochemistry of GFP

Formalin-fixed, paraffin-embedded tissue sections were first deparaffinized and rehydrated, followed by antigen retrieval using a citrate buffer (pH 6.0) at 95°C for 20 min. To block endogenous peroxidase activity, sections were treated with 3% hydrogen peroxide for 10 min and subsequently incubated with 5% BSA for 30 min at room temperature to prevent nonspecific binding. The sections were then incubated overnight at 4°C with a primary anti-GFP antibody (1:250 dilution; GeneTex, GTX113617). After thorough washing, samples were treated with a biotinylated secondary antibody, followed by incubation with horseradish peroxidase-conjugated streptavidin. Signal detection was carried out

Table 1 List of monoclone antibodies for flow cytometry

Reagent	DYE	Source	Identifier
Anti-mouse CD8a (clone 53–6.7)	PerCP/Cy5.5 BV785	BioLegend BioLegend	Cat#100733 Cat#100750
Anti-mouse granzyme B (clone GB11)	FITC Alexa 647	BioLegend BioLegend	Cat# 515403 Cat# 515405
Anti-mouse CD19 (clone 6D5)	PE/Dazzle594	BioLegend	Cat# 115553
Anti-mouse LAG-3 (clone C9B7W)	APC	eBioscience	Cat# 17–2231-82
Anti-mouse CD69 (clone H1.2F3)	APC Alexa 700 BV605	BioLegend BioLegend BioLegend	Cat# 104513 Cat# 104539 Cat# 104529
Anti-mouse Ki67 (clone 16A8)	APC	BioLegend	Cat# 652405
Anti-mouse Ki67 (clone B56)	BUV395	BD	Cat# 564071
Anti-mouse TCF-7/TCF-1 (clone S33-966)	R718	BD	Cat# 567587
Anti-mouse CD4 (clone GK1.5)	Alexa 700 Spark Blue 550 BV605	BioLegend BioLegend BD	Cat# 100430 Cat# 100473 Cat# 743156
Anti-mouse NK1.1 (clone PK136)	APC/Cy7 BV650	BioLegend BD	Cat# 108723 Cat# 564143
Anti-mouse CD11a (clone M17/4)	PE	BioLegend	Cat# 101107
Anti-mouse Perforin (clone S16009A)	PE PE/Dazzle594	BioLegend BioLegend	Cat# 154305 Cat# 154315
Anti-mouse TNF (clone MP6-XT22)	BV650	BD	Cat# 563943
$H2K^b$/SIINFEKL (clone JD02163)	PE	Immudex	Cat# NC1679807
Anti-mouse PD-1 (clone J43)	BUV737	BD	Cat# 568362
Anti-mouse PD-1 (clone 29F.1A12)	PE	BioLegend	Cat# 135205
Anti-mouse PD-1 (clone RMP1-30)	PE/Dazzle594 BUV737	BioLegend BioLegend	Cat# 109115 Cat# 568362
Anti-mouse CX3CR1 (clone SA011F11)	Spark PLUS UV395	BioLegend	Cat# 149065
Anti-mouse KLRG1 (clone 2F1/KLRG1)	PerCP/Cy5.5	BioLegend	Cat# 138417
Anti-mouse CD49a (clone Ha31/8)	BV711	BD	Cat# 564863
Anti-mouse CD3 (clone 145–2 C11)	PE/Cy7 BV711 Spark YG 593	BioLegend BD BioLegend	Cat# 100319 Cat# 563123 Cat# 100373
Anti-mouse CD3 (clone 17-A2)	APC/Fire810	BioLegend	Cat# 100267
Anti-mouse IFN-γ (clone XMG1.2)	PE/Cy7 Spark NIR 685	BioLegend BioLegend	Cat# 505825 Cat# 505861
Anti-mouse FasL (clone MFL3)	APC	BioLegend	Cat# 106609
Anti-mouse CD107a (clone 1D4B)	BV421	BioLegend	Cat# 121617
Anti-mouse CD127 (clone A7R34)	BV421 PE/Cy5	BD BioLegend	Cat# 566377 Cat# 135015
Anti-mouse Tim3 (clone 5D12)	BV421	BD	Cat# 747626
Anti-mouse Tim3 (clone RMT3-23)	PE/Fire 810	BioLegend	Cat# 119745
Anti-mouse Ly108 (clone 330-AJ)	PE	BioLegend	Cat# 134605
Anti-mouse CD45 (clone 30-F11)	BV510	BD	Cat# 563891
Anti-mouse CD25 (clone PC61)	BV605	BD	Cat# 563061
Anti-mouse CD44 (clone IM7)	BV786	BD	Cat# 563736
Zombie Green Fixable Viability Kit	FITC	BioLegend	Cat# 423112
Zombie UV Fixable Viability Kit	UV	BioLegend	Cat# 423107
Zombie Red Fixable Viability Kit	PE/Dazzle594	BioLegend	Cat# 423109

Continued

Table 1 Continued

Reagent	DYE	Source	Identifier

APC, Allophycocyanin; mAbs, monoclone antibodies; PE, Phycoerythrin; RT-qPCR, real-time quantitative PCR; Tcircm, circulating memory T cells; Teff, effector T cells; Tintex, intermediate exhausted T cells; Tm, memory T cells; Tpex, progenitor exhausted T cells; Ttex, terminally exhausted T cells.

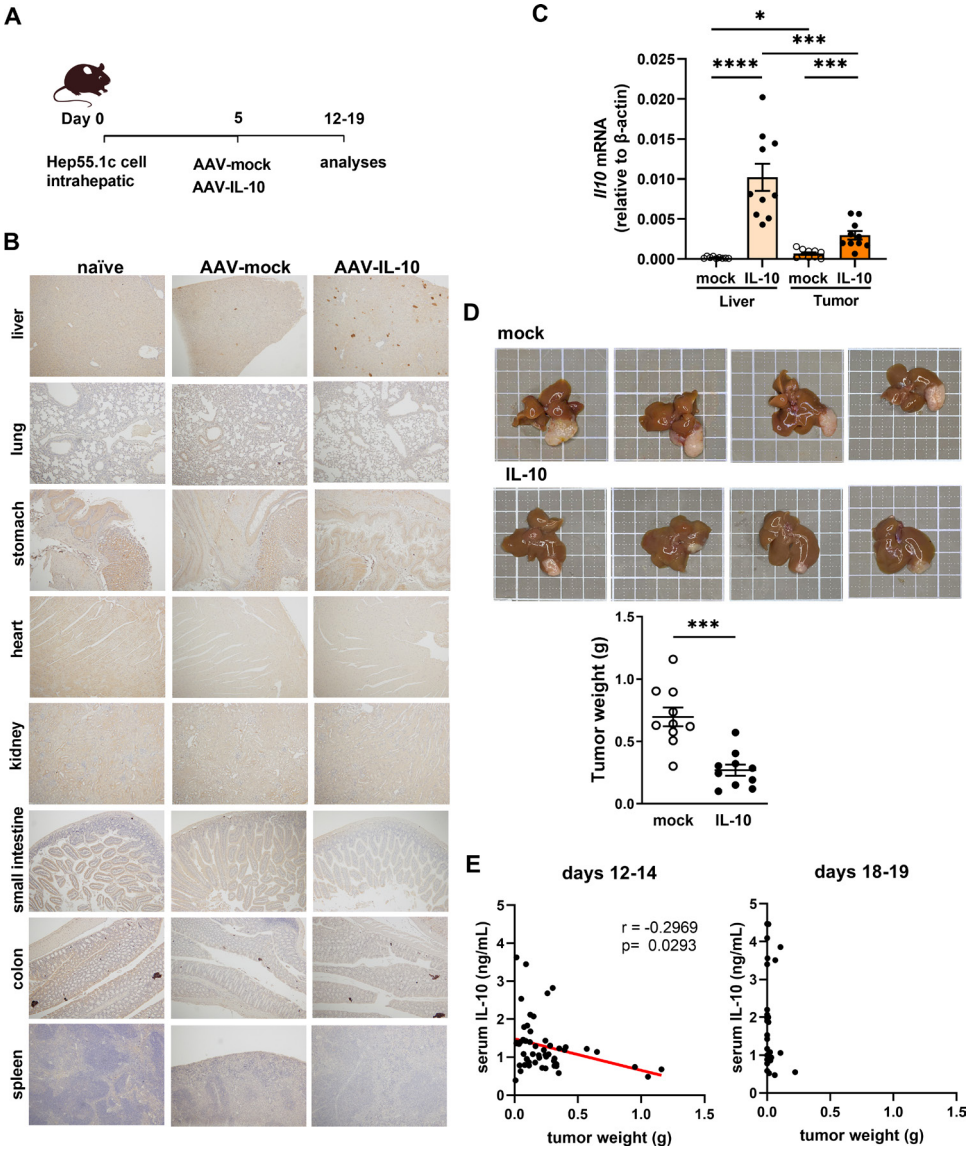

Figure 1 AAV-IL-10 treatment inhibited liver tumor growth. Hep55.1c tumor cells were intrahepatically inoculated into C57BL/6 mice on day 0. 5 days later, mice received an intravenous injection of either AAV-IL-10 or AAV-mock. (A) Experimental timeline. (B) AAV expression in different organs was evaluated by immunohistochemistry using an anti-GFP antibody. A naïve mouse was included as a negative control. Brown staining indicates GFP-positive cells (×100 magnification). (C) *Il10* expression levels in liver and tumor tissues were quantified by RT-qPCR, with data analyzed using the $2^{-\Delta Ct}$ relative to β-actin. (D) Representative macroscopic images of liver tumors and tumor weights of AAV-IL-10 and AAV-mock treated tumor bearing mice on day 14. (E) Correlation between serum IL-10 levels and tumor weights in AAV-IL-10-treated tumor bearing mice was evaluated on days 12–14 and 18–19. Each dot represents an individual mouse. All error bars denote±SEM. *p<0.05; ***p<0.001; ****p<0.0001. AAV, adeno-associated virus; IL, interleukin; GFP, green fluorescent protein; RT-qPCR, real-time quantitative PCR.

using 3,3'-diaminobenzidine as the chromogen, and the sections were counterstained with hematoxylin.

RT-qPCR of IL-10 and chemokines

Tumor specimens were used for total RNA extraction using the NucleoSpin RNA kit (Macherey-Nagel), followed by DNase treatment to remove potential genomic DNA contamination. Complementary DNA (cDNA) was synthesized using oligonucleotide primers and the High-Capacity cDNA Reverse Transcription Kit (Applied Biosystems). QPCR was performed with SYBR Green Master Mix (Thermo Scientific) on the 7500 Real-Time PCR System (Applied Biosystems). Gene expression levels were analyzed using the $2^{-\Delta Ct}$ relative quantification method, with normalization to β-actin as the internal control. The primer sequences used in the qPCR analysis were as follows: *Actb* (forward: CAC AGT GTT GTC TGG TGG TA; reverse: GAC TCA TCG TAC TCC TGC TT), *Il10* (forward: GGT TGC CAA GCC TTA TCG GA; reverse: ACC TGC TCC ACT GCC TTG CT), *Ccl5* (forward: AGA TCT CTG CAG CTG CCC TCA; reverse: GGA GCA CTT GCT GCT GGT GTA G), *Ccl19* (forward: CTG CCT CAG ATT ATC TGC CAT; reverse: AGG TAG CGG AAG GCT TTC AC), *Cxcl9* (forward: CGA TCC ACT ACA AAT CCC TCA; reverse: AGT CCG GAT CTA GGC AGG TT), *Cxcl10* (forward: GGA TGG CTG TCC TAG CTC TG; reverse: TGA GCT AGG GAG GAC AAG GA), and *Cxcl16* (forward: ACC CTT GTC TCT TGC GTT CTT CCT; reverse: ATG TGA TCC AAA GTA CCC TGC GGT).

Statistical analysis

Data are presented as the mean±SEM. Statistical analysis was performed using a two-tailed unpaired Student's t-test. A p-value of <0.05 was considered statistically significant. All analyses were conducted using Prism V.9 software (GraphPad Software).

RESULTS

AAV-IL-10 treatment suppressed tumor growth

To assess the potential of liver-directed IL-10 delivery in suppressing liver tumor progression, C57BL/6 mice received a single intravenous injection of IL-10-expressing AAV (AAV-IL-10) or control vector (AAV-mock) 5 days after orthotopic inoculation with Hep55.1c tumor cells (figure 1A). Immunohistochemical analysis revealed that IL-10 expression following AAV-IL-10 administration was predominantly localized in the liver, with no detectable expression in other organs (figure 1B). IL-10 messenger RNA was detected in both liver and tumor tissues of AAV-IL-10-treated mice, with higher expression in the liver compared with the tumor (figure 1C). This likely reflects more efficient AAV transduction in hepatocytes than in Hep55.1c tumor cells, as well as the non-replicating nature of AAV vectors, which limits transgene persistence in rapidly dividing tumor cells relative to stable hepatocytes. Tumor analysis conducted 14 days post-inoculation revealed a significant reduction in tumor weight in AAV-IL-10-treated mice (figure 1D). Furthermore, tumor weight negatively correlated with serum IL-10 levels in AAV-IL-10-treated mice on days 12–14 post-inoculation. By days 18–19, tumors were notably smaller or undetectable in 50% (14 out of 28) of the AAV-IL-10-treated mice (figure 1E). Collectively, these findings demonstrate that liver-directed AAV-IL-10 therapy effectively suppresses liver tumor growth.

AAV-IL-10 enhances CD8$^+$ T cell-mediated antitumor responses

Analysis of tumor-infiltrating immune cells revealed a significant increase in the absolute number of CD45$^+$ cells following AAV-IL-10 treatment (figure 2A). Further characterization of effector cell subsets in tumor-infiltrating leukocytes revealed that AAV-IL-10 treatment significantly increased both the percentage and absolute number of CD8$^+$ T cells within the tumor microenvironment. In contrast, the frequencies of natural killer (NK) cells and CD4$^+$ T cells were decreased, while their absolute numbers remained unchanged (figure 2B–D). Additionally, the expression of T cell-attracting chemokines, including *Ccl5*, *Ccl19*, *Cxcl9*, *Cxcl10*, and *Cxcl16*, was significantly elevated in the IL-10-treated liver microenvironment (figure 2E). To assess the contribution of CD8$^+$ T cells to the antitumor effects of AAV-IL-10, we performed CD8$^+$ T-cell depletion experiments. Anti-CD8 antibody was administered starting 1 day prior to AAV-IL-10 treatment and continued until the end of the experiment. Seven mice were initially enrolled in the CD8$^+$ T-cell depletion group; however, three animals reached humane endpoints or died before the planned experimental endpoint and were therefore excluded from the final analysis. CD8$^+$ T cells were undetectable in the depletion group, confirming effective CD8$^+$ T-cell depletion (figure 2F). CD8$^+$ T-cell depletion was associated with increased body weight loss and higher tumor burden compared with AAV-IL-10-treated mice receiving isotype control antibody (figure 2G,H). Notably, body weight loss did not strictly correlate with tumor weight in this cohort (data not shown). Together, these data provide supportive evidence that CD8$^+$ T cells contribute to the antitumor effects of AAV-IL-10, while acknowledging the limited statistical power of this experiment.

To further investigate whether IL-10 exerts a direct effect on tumor cells, we examined IL-10 receptor expression on Hep55.1c cells cultured with or without recombinant IL-10. We found that Hep55.1c cells did not express IL-10 receptor under any tested condition (data not shown), suggesting that IL-10 does not directly influence tumor cell growth or survival.

AAV-IL-10 treatment enhanced the functional activity of tumor-infiltrating NK and CD8$^+$ T cells

To assess the impact of AAV-IL-10 on the functional activity of tumor-infiltrating immune cells, we analyzed

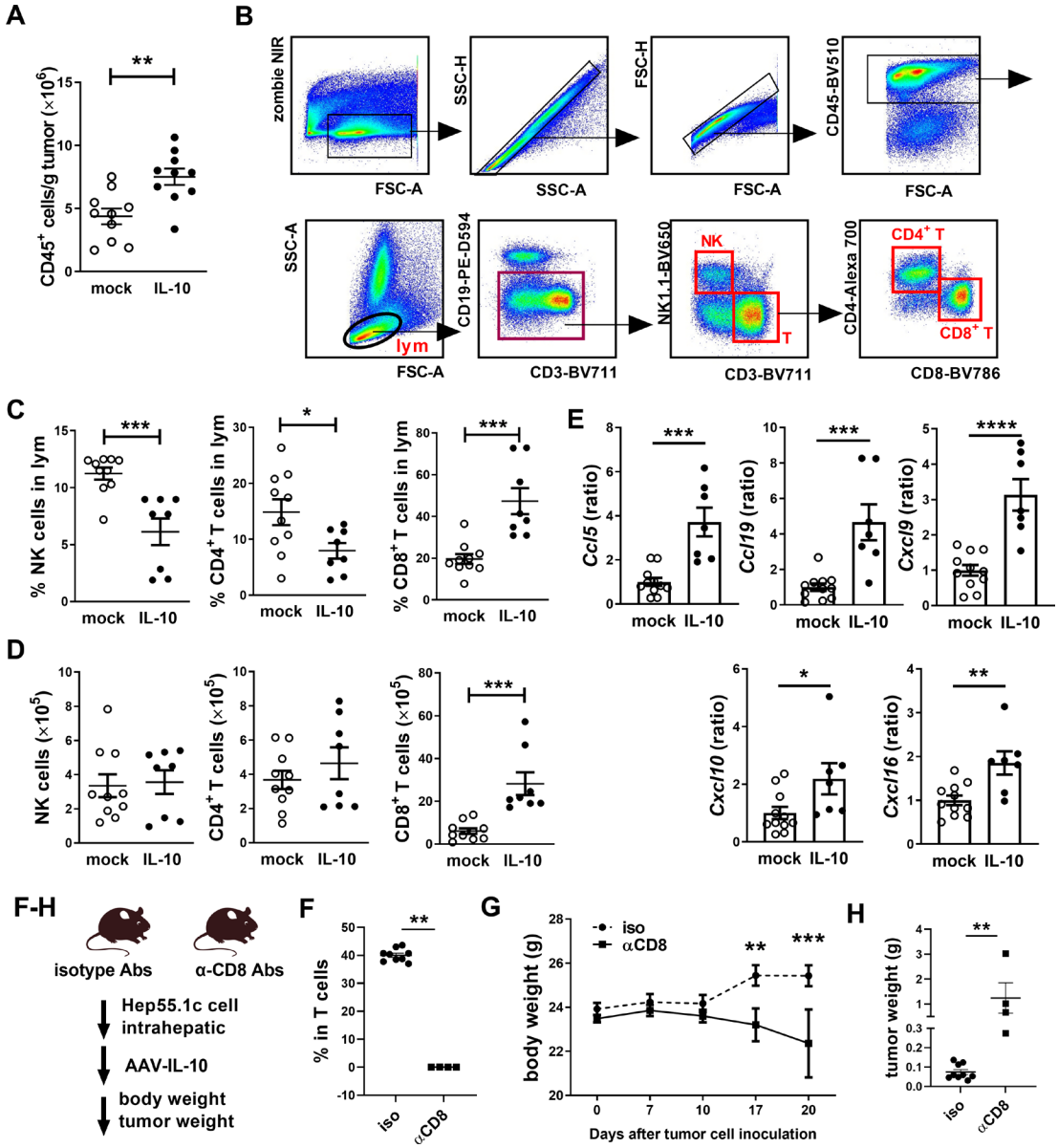

Figure 2 AAV-IL-10 enhances intratumoral CD8$^+$ T-cell infiltration and mediates antitumor immunity. Mice were inoculated with Hep55.1c tumor cells and treated with AAV-IL-10 as described in figure 1A. Tumor-infiltrating immune cells were analyzed by flow cytometry on day 14. (A) Quantification of CD45$^+$ tumor-infiltrating leukocytes per gram of tumor tissue. (B) Representative flow-cytometry plots illustrating gating strategies for lymphocyte subsets within tumors. (C) Percentages of NK cells, CD4$^+$ T cells, and CD8$^+$ T cells among total tumor-infiltrating lymphocytes. (D) Absolute numbers of NK cells, CD4$^+$ T cells, and CD8$^+$ T cells per gram of tumor. (E) Relative expression of chemokine genes in tumor tissues assessed by RT-qPCR and normalized to the AAV-mock group (set as 1). (F–H) CD8$^+$ T-cell depletion was performed using anti-CD8 antibodies or isotype control antibodies administered two times a week beginning 1 day before AAV treatment. (F) Percentages of CD8$^+$ T cells among total T cells were measured 1 day after antibody administration by flow cytometry. (G) Body weights of mice were monitored throughout the experiment. (H) Tumor weights of AAV-IL-10-treated, anti-CD8-treated or isotype-treated tumor-bearing mice at endpoint. Each dot represents a pooled sample from one to three mice. All error bars denote±SEM. *p<0.05; **p<0.01; ***p<0.001; ****p<0.0001. AAV, adeno-associated virus; IL, interleukin; NK, natural killer; RT-qPCR, real-time quantitative PCR.

cytokine and cytotoxic molecule expression in NK and CD8$^+$ T cells. AAV-IL-10 treatment significantly increased the percentages of NK cells expressing IFN-γ, TNF-α, and granzyme B compared with AAV-mock treatment (figure 3A). In addition, the proportion of multifunctional NK cells was elevated following AAV-IL-10 administration (figure 3B). Similarly, CD8$^+$ T cells from AAV-IL-10-treated mice exhibited enhanced expression of IFN-γ, and granzyme B relative to controls (figure 3C), and the proportion of multifunctional CD8$^+$ T cells was also increased (figure 3D). Collectively, these results demonstrate that AAV-IL-10 enhances antitumor immunity by increasing CD8$^+$ T-cell infiltration and promoting the effector

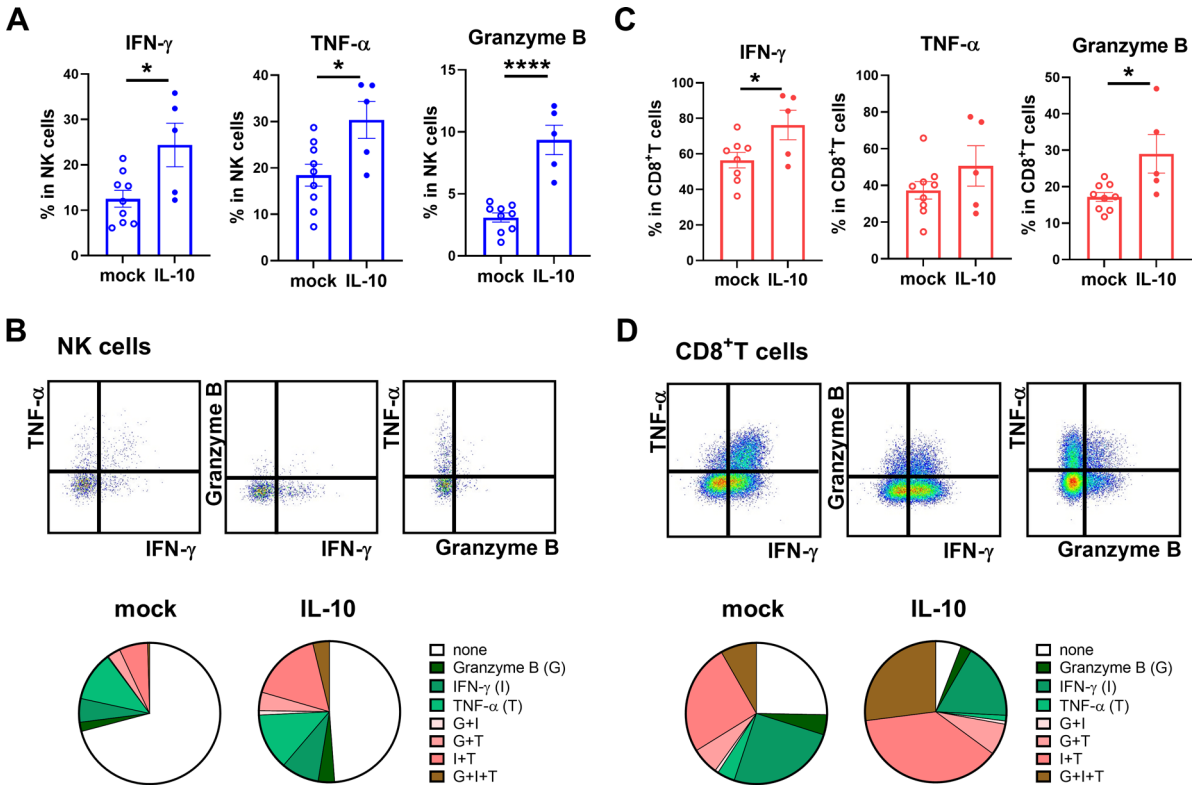

Figure 3 AAV-IL-10 treatment enhanced the functional activity of tumor-infiltrating NK and CD8$^+$ T cells. Mice were inoculated with tumor cells and treated with AAV-IL-10 as described in figure 1A. On day 14, tumor-infiltrating cells were isolated and stimulated with PMA and ionomycin for 2 hours. Effector molecule expression was analyzed by flow cytometry. (A) Expression of IFN-γ, TNF-α, and granzyme B in NK cells. (B) Representative flow cytometry plots and proportions of NK cells expressing none, one, two, or all three effector molecules (IFN-γ, TNF-α, and granzyme B). (C) Expression of IFN-γ, TNF-α, and granzyme B in CD8$^+$ T cells. (D) Representative flow cytometry plots and proportions of CD8$^+$ T cells expressing none, one, two, or all three effector molecules (IFN-γ, TNF-α, and granzyme B). Each dot represents a pooled sample from one to three mice. All error bars denote±SEM. *p<0.05; ****p<0.0001. AAV, adeno-associated virus; IFN, interferon; IL, interleukin; NK, natural killer; PMA, phorbol-12-myristate-13-acetate; TNF, tumor necrosis factor.

functions of both NK and CD8$^+$ T cells within the tumor microenvironment.

AAV-IL-10 enhanced the effector functions of terminally exhausted CD8$^+$ TILs

Within the tumor microenvironment, chronic exposure to tumor antigens drives CD8$^+$ T cells toward an exhausted state.[27] This exhaustion is widely regarded as a progressive differentiation process. Based on the expression of T-cell factor-1 (TCF-1), T-cell immunoglobulin and mucin domain-containing protein 3 (TIM-3), and programmed cell death protein 1 (PD-1), exhausted CD8$^+$ T cells can be categorized into distinct subsets: progenitor (TCF-1$^+$TIM-3$^-$), intermediate (TCF-1$^-$TIM-3$^-$), terminally exhausted (TCF-1$^-$TIM-3$^+$PD-1$^+$), and effector-like (TCF-1$^-$TIM-3$^+$PD-1$^-$) cells.[28] To investigate whether AAV-IL-10 modulates antigen-specific CD8$^+$ T-cell exhaustion in HCC, we used OVA-expressing Hep55.1c tumors and identified OVA-specific CD8$^+$ TILs using an H-2K^b-restricted OVA$_{257–264}$ tetramer. Given the limited number of TILs recovered from tumors and the low frequency of OVA-specific CD8$^+$ T cells within the total CD8$^+$ TIL pool, we assessed effector function using PMA/ionomycin stimulation in combination with tetramer labeling. This approach enabled simultaneous evaluation of the effector potential of both tumor antigen-specific and bystander CD8$^+$ T cells, providing an integrated view of intratumoral CD8$^+$ T-cell activation following AAV-IL-10 treatment. The frequencies of OVA-specific CD8$^+$ TILs between AAV-mock and AAV-IL-10 administered HCC-bearing mice were comparable (figure 4A). In the AAV-mock-treated HCC model, approximately 20.3% of OVA-specific CD8$^+$ TILs were terminally exhausted, while only ~7.6% remained in the progenitor exhausted state. In contrast, among non-OVA-specific CD8$^+$ TILs, ~10.7% were terminally exhausted and ~28.4% were progenitor exhausted, indicating that tumor antigen (OVA)-specific CD8$^+$ T cells exhibited a more pronounced terminal exhaustion phenotype. AAV-IL-10 treatment did not alter the exhaustion state of OVA-specific CD8$^+$ TILs, while it promoted non-OVA-specific CD8 T cells to intermediate state (figure 4B). Notably, AAV-IL-10 treatment significantly enhanced the expression of key effector molecules, IFN-γ and granzyme B, in terminally exhausted OVA-specific CD8$^+$ TILs (figure 4C).

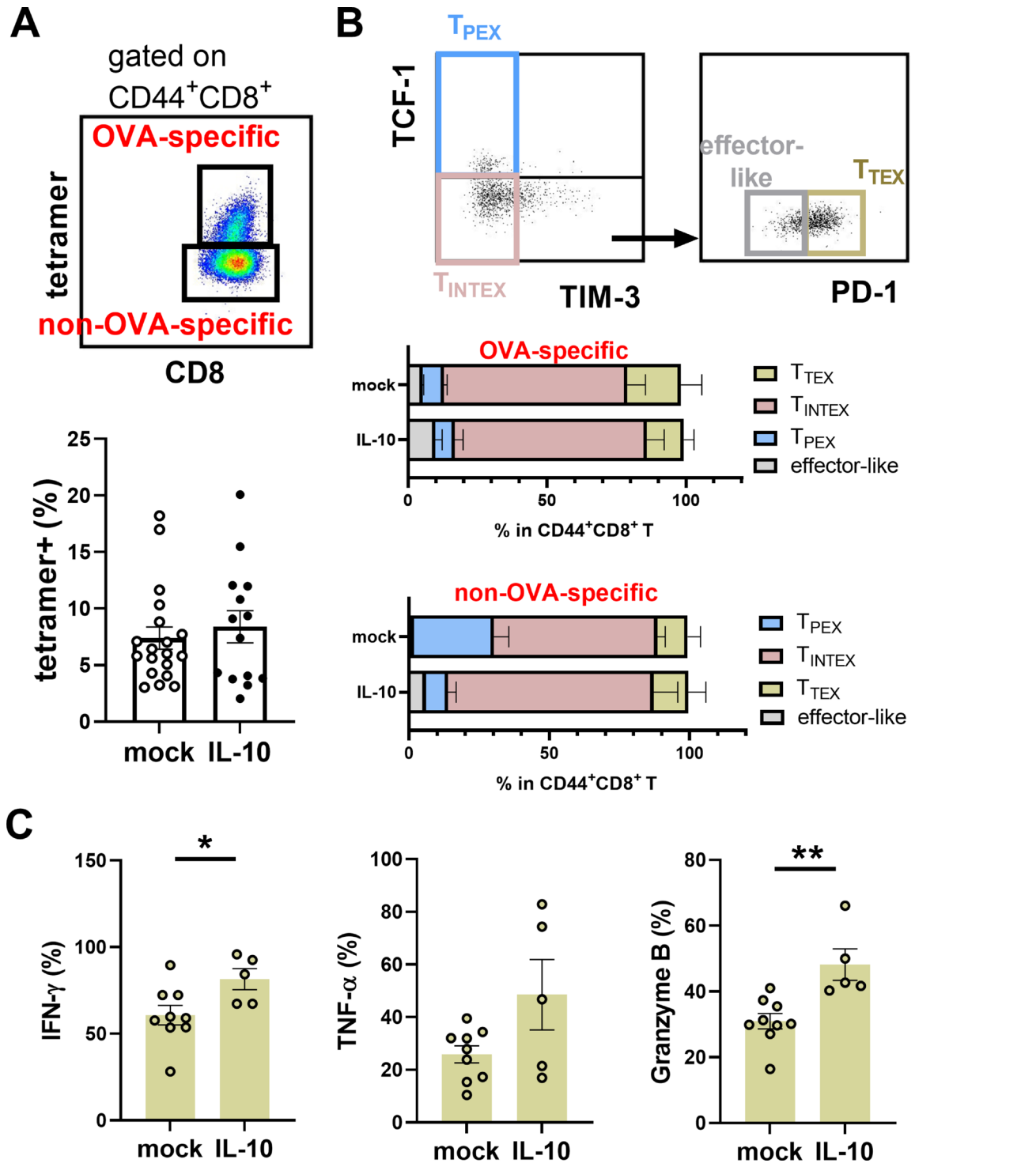

Figure 4 AAV-IL-10 enhanced the effector functions of terminally exhausted CD8$^+$ TILs. Mice were inoculated with Hep55.1c-OVA and treated with AAV-IL-10 as described in figure 1A. On day 14, tumor-infiltrating cells were isolated, and exhausted CD8$^+$ T cells along with their effector molecule expression were analyzed. (A) The representative flow cytometry plot and graphical summary showing the frequency of OVA-specific CD8$^+$ T cells. (B) Representative flow cytometry plots showing the gating strategy of effector-like cells, progenitor, intermediate, and terminally exhausted CD8$^+$ T cells (T_{PEX}, T_{INTEX}, and T_{TEX}, respectively) from OVA-specific and non-OVA-specific CD8$^+$ T cells in (A). Graphical summary showing the proportions of effector-like, T_{PEX}, T_{INTEX}, and T_{TEX} cells in OVA-specific and non-OVA-specific CD8$^+$ T cells. T_{PEX} were identified as TCF-1$^+$TIM-3$^-$, T_{INTEX} were TCF-1$^-$TIM-3$^-$, while terminally T_{TEX} were TCF-1$^-$TIM-3$^+$PD-1$^+$, and effector-like cells were TCF-1$^-$TIM-3$^+$PD-1$^-$. Four to five mice per group were included in the summary plot. (C) Expression of effector molecules in OVA-specific CD8$^+$ T_{TEX}. Each dot represents a pooled sample from one to three mice. All error bars denote±SEM. *p<0.05; **p<0.01. AAV, adeno-associated virus; IFN, interferon; IL, interleukin; OVA, ovalbumin; PD-1, programmed cell death protein 1; TCF-1, T-cell factor-1; TIM-3, T-cell immunoglobulin and mucin domain-containing protein 3; TNF, tumor necrosis factor; T_{PEX}, progenitor exhausted CD8$^+$ T cells; T_{INTEX}, intermediate exhausted CD8$^+$ T cells; T_{TEX}, terminally exhausted CD8$^+$ T cells.

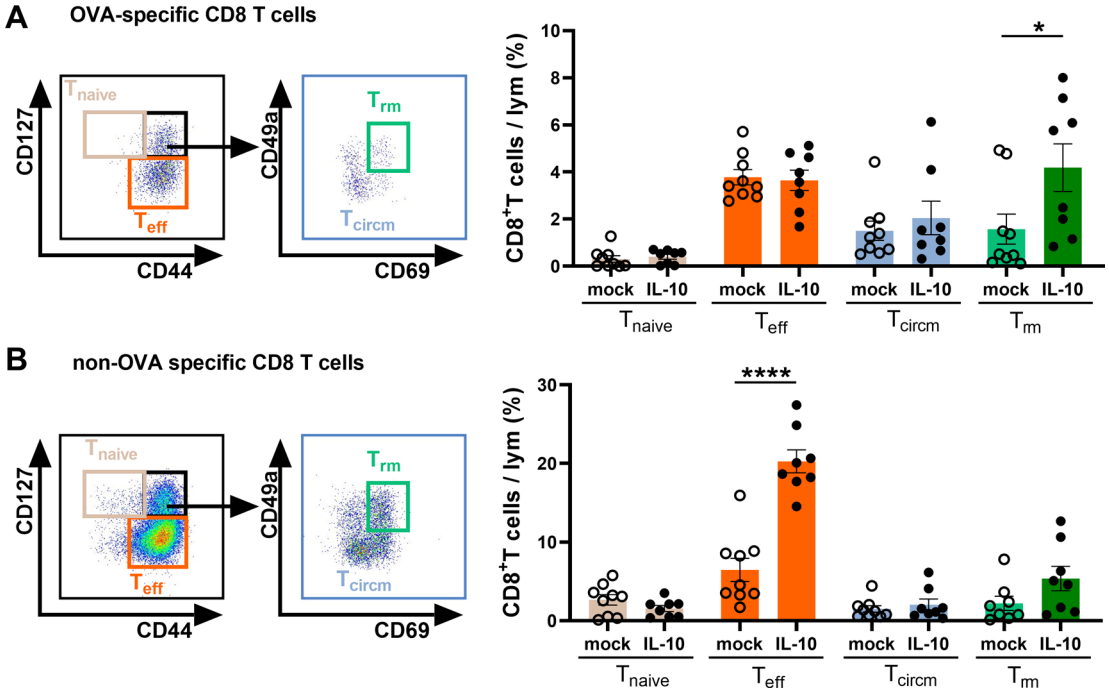

Figure 5 AAV-IL-10 treatment increased CD8$^+$ T cells with a Trm cell phenotype within tumor. Mice were inoculated with Hep55.1c-OVA tumor cells and treated with AAV-IL-10 as described in figure 1A. On day 14, tumor-infiltrating cells were isolated, and CD8$^+$ T-cell subsets were analyzed by flow cytometry. (A) Representative flow cytometry plots and graphical summary depicting the frequency of OVA-specific CD8$^+$ T-cell subsets. (B) Representative flow cytometry plots and graphical summary illustrating the frequency of non-OVA-specific CD8$^+$ T-cell subsets. Each dot represents a pooled sample from one to three mice. All error bars denote±SEM. *p<0.05; ****p<0.0001. AAV, adeno-associated virus; IL, interleukin; OVA, ovalbumin; Tnaive, naive T cells; Teff, effector T cells; Tcircm, circulating memory T cells; Trm, tissue-resident memory T cells.

AAV-IL-10 treatment increased CD8$^+$ T cells with a Trm cell phenotype within tumor

To further characterize the phenotype of tumor-infiltrating CD8$^+$ T cells, we categorized CD8$^+$ TILs into four subsets based on the expression of CD127, CD44, CD69, and CD49a. AAV-IL-10 treatment significantly increased both the CD127$^-$CD44$^+$ effector and CD127$^+$CD44$^+$CD69$^+$CD49a$^+$ Trm phenotypes of CD8$^+$ TILs. Notably, the expansion of CD127$^+$CD44$^+$CD69$^+$CD49a$^+$ CD8$^+$ Trm-like cells was predominantly observed within the OVA-specific subset (figure 5A), whereas the increase in the effector subtype was more pronounced among non-OVA-specific CD8$^+$ TILs (figure 5B).

CD8$^+$ Trm-like cells in the HCC tumor model are liver-resident and long-lasting

Because AAV-IL-10 treatment significantly increased the frequency of CD127$^+$CD44$^+$CD69$^+$CD49a$^+$ CD8$^+$ Trm-like cells in the liver, we next sought to determine whether these cells were truly tissue-resident rather than replenished from circulating lymphocytes. To test this, we administered FTY720—a sphingosine-1-phosphate receptor modulator that prevents lymphocyte egress from LNs in untreated HCC-bearing mice[29] (figure 6A). As expected, FTY720 treatment markedly reduced circulating leukocyte counts (figure 6B), confirming effective blockade of lymphocyte trafficking. Despite this reduction, the abundance of intratumoral CD127$^+$CD44$^+$CD69$^+$CD49a$^+$ CD8$^+$ Trm-like cells remained unchanged following FTY720 treatment, and these cells were virtually undetectable in the draining LNs (figure 6C). These findings indicate that CD127$^+$CD44$^+$CD69$^+$CD49a$^+$ CD8$^+$ cells are maintained locally within the liver and are not replenished from recirculating pools. Moreover, a substantial proportion of intratumoral CD8$^+$ Trm-like cells expressed Ki67, regardless of FTY720 treatment, demonstrating their proliferative potential within the hepatic microenvironment (figure 6D). Together, these results confirm that the CD8$^+$ Trm-like population observed in this HCC model represents a liver-resident and self-sustaining subset.

To investigate their long-term persistence, we assessed CD8$^+$ Trm-like cells on day 56 in AAV-IL-10-treated, tumor-free mice (figure 6E). While no visible tumors were present in the liver, OVA-specific CD8$^+$ Trm-like cells persisted, and Trm-like cells remained the dominant CD8$^+$ subset in the liver of these tumor-free mice (figure 6F). Collectively, these findings indicate that CD127$^+$CD44$^+$CD49a$^+$CD69$^+$ CD8$^+$ T cells in this model are liver-resident, proliferative, and exhibit long-term memory characteristics.

AAV-IL-10 suppresses metastatic liver tumor growth and enhances infiltration of CD8$^+$ Trm-like cells

We next evaluated whether AAV-IL-10 administration could suppress the growth of metastatic liver tumors. To establish an intrahepatic metastasis model of HCC, Hep55.1c-OVA cells were injected into the spleen of C57BL/6 mice. Mice subsequently received intravenous

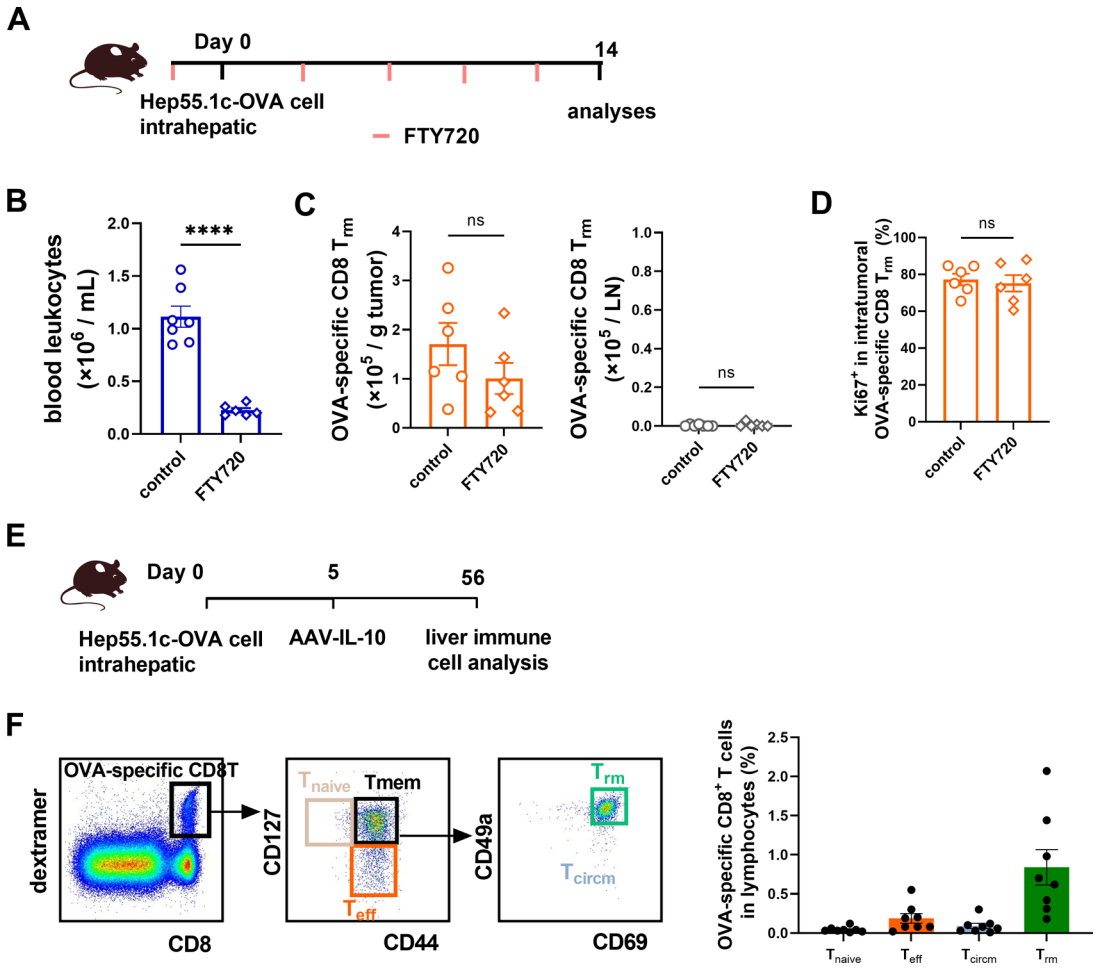

Figure 6 CD8$^+$ Trm-like cells in the HCC tumor model were liver-resident and long-lasting. Hep55.1c-OVA tumor cells were intra-hepatically inoculated into C57BL/6 mice on day 0. (A–D) FTY720 was administered starting 1 day before tumor inoculation and continued every 2 days until day 13. No AAV-IL-10 or AAV-mock was administered in the experiments. On day 14, peripheral blood, draining LNs, and tumor tissues were collected for analysis. (A) Experimental timeline. (B) Quantification of peripheral leukocytes. (C) Analysis of OVA-specific CD8$^+$ Trm-like cells in the tumor and draining LNs. (D) Proliferation of intratumoral OVA-specific CD8$^+$ Trm-like cells. (E–F) Mice were treated with AAV-IL-10 and CD8$^+$ Trm-like cells in livers were detected on day 56. (E) Experimental timeline. (F) Representative flow cytometry plots and graphical summary showing the frequency of OVA-specific CD8$^+$ T-cell subsets. Each dot represents an individual mouse. All error bars denote±SEM. ****p<0.0001. AAV, adeno-associated virus; HCC, hepatocellular carcinoma; IL, interleukin; LN, lymph node; OVA, ovalbumin; Tnaive, naive T cells; Teff, effector T cells; Tcircm, circulating memory T cells; Trm, tissue-resident memory T cells.

injections of AAV-IL-10 or AAV-mock, after which liver tumor burden and immune cell infiltration were analyzed (figure 7A). As shown in figure 7B, prominent tumor nodules were observed in AAV-mock-treated mice, whereas liver tumors were largely undetectable in AAV-IL-10-treated mice. Consistently, liver weights were significantly reduced in the AAV-IL-10-treated group compared with controls (p<0.01; figure 7B). AAV-IL-10 treatment markedly increased both the frequency and absolute number of intrahepatic CD8$^+$ T cells (figure 7C,D). In addition, AAV-IL-10 significantly enhanced CD8$^+$ T-cell effector function, as evidenced by increased frequencies of IFN-γ-producing CD8$^+$ T cells and elevated expression of granzyme B and IFN-γ compared with AAV-mock treatment (figure 7E). Similarly, NK cells from AAV-IL-10-treated mice exhibited higher expression of IFN-γ and granzyme B relative to controls (figure 7F). Notably, AAV-IL-10 treatment also led to a significant expansion of OVA-specific CD8$^+$ Trm-like cells in the intrahepatic metastatic HCC model (figure 7G).

Liver-directed AAV-IL-10 treatment does not suppress distant subcutaneous tumor growth

To assess the tissue specificity of liver-directed AAV-IL-10 therapy, we inoculated Hep55.1c cells subcutaneously into the right leg of mice and administered AAV-IL-10 5 days later (figure 8A). Serum IL-10 levels on day 14 after tumor inoculation were detectable and comparable to those observed in the orthotopic HCC model (figure 8B). However, IL-10 and GFP expression were markedly lower in tissues surrounding subcutaneous tumors compared with the liver (figure 8C). Consistent with this, AAV-IL-10 treatment did not reduce subcutaneous tumor size or weight (figure 8D,E). Furthermore, the total number

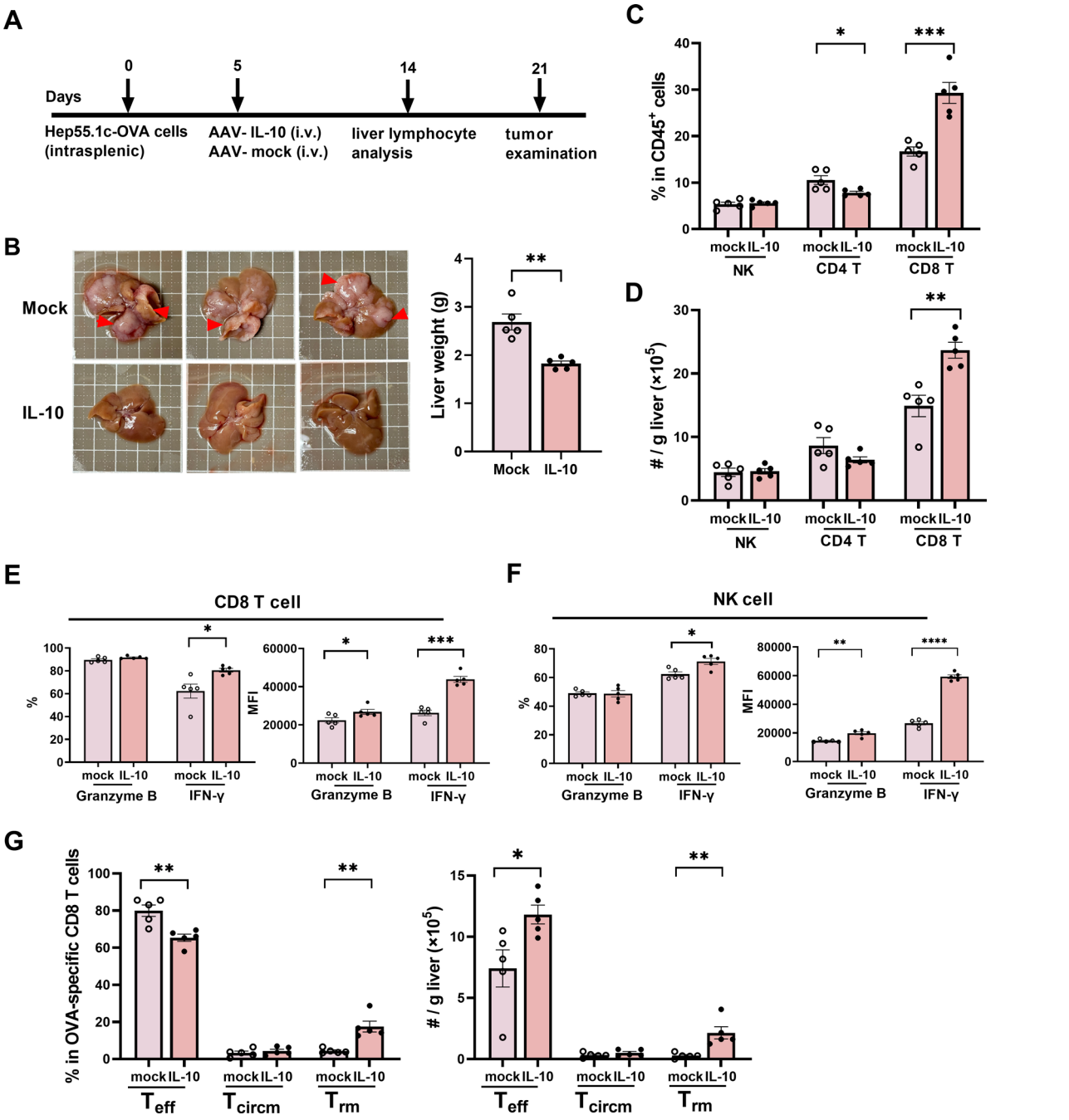

Figure 7 AAV-IL-10 suppresses metastatic liver tumor growth and enhances CD8$^+$ Trm-like cell infiltration. Hep55.1c-OVA tumor cells were intrasplenically inoculated into C57BL/6 mice on day 0.5 days later, mice received an intravenous injection of either AAV-IL-10 or AAV-mock. (A) Experimental timeline. (B) Representative macroscopic images of livers showing tumor burden, along with liver weights, from AAV-IL-10-treated and AAV-mock-treated tumor-bearing mice on day 21. (C–G) Liver leukocytes were analyzed by flow cytometry on day 14. (C) Percentages of NK cells, CD4$^+$ T cells, and CD8$^+$ T cells among total liver leukocytes. (D) Absolute numbers of NK cells, CD4$^+$ T cells, and CD8$^+$ T cells per gram of liver tissue. (E, F) Liver leukocytes were stimulated with PMA and ionomycin for 2 hours, followed by flow cytometric analysis of granzyme B and IFN-γ expression in CD8$^+$ T cells (E) and NK cells (F). (G) Frequencies and absolute numbers of OVA-specific CD8$^+$ T-cell subsets. Each dot represents an individual mouse. All error bars denote mean±SEM. *p<0.05; **p<0.01; ***p<0.001; ****p<0.0001. AAV, adeno-associated virus; IFN, interferon; IL, interleukin; i.v., intravenous; MFI, mean fluorescence intensity; NK, natural killer; OVA, ovalbumin; PMA, phorbol-12-myristate-13-acetate; Teff, effector T cells; Tcircm, circulating memory T cells; Trm, tissue-resident memory T cells.

of CD45$^+$ tumor-infiltrating leukocytes, as well as CD4$^+$ and CD8$^+$ T cells, remained similar between AAV-mock-treated and AAV-IL-10-treated mice bearing subcutaneous tumors. Interestingly, NK cell numbers were reduced in the AAV-IL-10-treated group (figure 8F,G). These findings indicate that AAV-IL-10 exerts its immunomodulatory

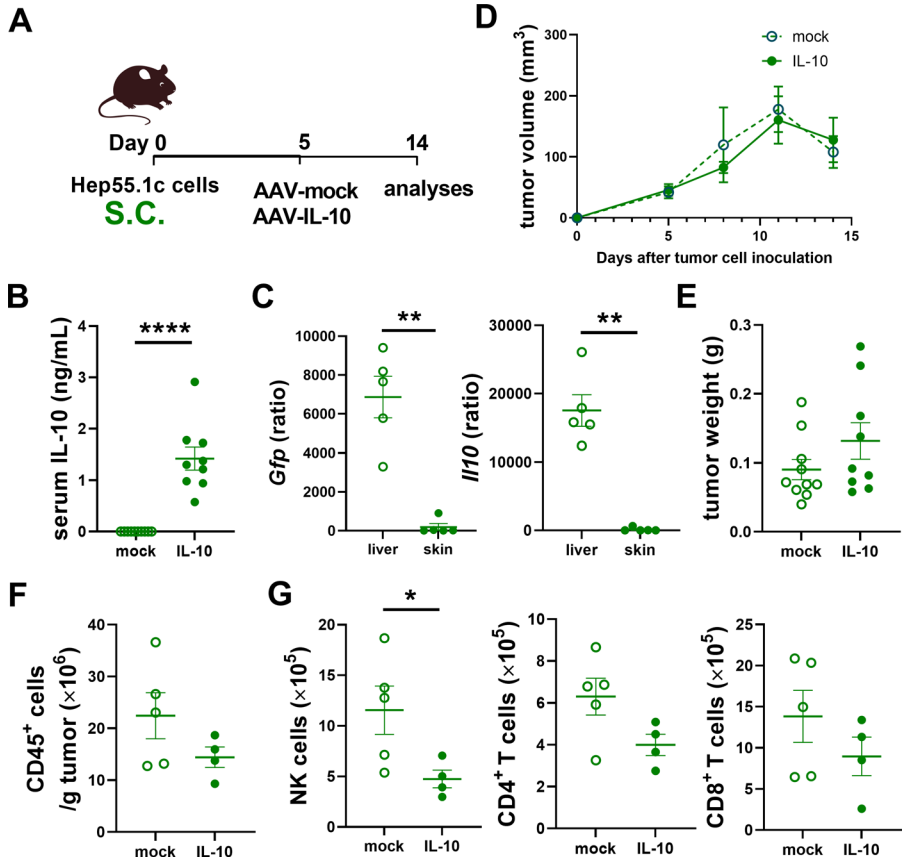

Figure 8 Liver-directed AAV-IL-10 treatment did not impact subcutaneous tumor growth. Hep55.1c tumor cells were subcutaneously (s.c.) inoculated into C57BL/6 mice on day 0. 5 days later, mice received an intravenous injection of either AAV-IL-10 or AAV-mock. (A) Experimental timeline. (B) Serum IL-10 concentrations were assessed on day 14. (C) *Gfp* and *Il10* expression levels in liver and skin tissues were quantified by RT-qPCR, with data analyzed using the $2^{-\Delta Ct}$ relative to β-actin. (D) Tumor volumes were monitored throughout tumor progression. (E) Tumor weights were measured on day 14. (F) $CD45^+$ tumor-infiltrating leukocytes were quantified per gram of tumor. (G) Absolute numbers of NK cells, $CD4^+$ T cells, and $CD8^+$ T cells within the tumor were determined. Each dot represents an individual mouse. All error bars denote±SEM. *p<0.05; **p<0.01; ****p<0.0001. AAV, adeno-associated virus; IL, interleukin; NK, natural killer; RT-qPCR, real-time quantitative PCR.

and antitumor effects specifically within the liver tumor microenvironment, without influencing distant tumor sites.

DISCUSSION

In this study, we evaluated the antitumor immune response of IL-10 in HCC using a syngeneic orthotopic HCC mouse model. To achieve liver-specific expression of IL-10, we employed a liver-directed AAV vector to deliver IL-10. Hep55.1c hepatoma cells were orthotopically implanted into the liver, followed by intravenous administration of either AAV-IL-10 or a control vector (AAV-mock). Mice treated with AAV-IL-10 exhibited a significant reduction in tumor burden, accompanied by a pronounced increase in TILs, particularly $CD8^+$ T cells. These $CD8^+$ T cells demonstrated enhanced cytotoxic activity, as indicated by elevated expression of effector molecules such as IFN-γ and granzyme B. Notably, IL-10 treatment induced a population of CD8 Trm phenotype TILs, which persisted within the liver over the long-term. Furthermore, this therapeutic approach selectively targeted liver tumors without affecting distant subcutaneous tumors. Collectively, these findings underscore the potential of liver-directed AAV-IL-10 as an immunotherapeutic strategy for HCC by enhancing $CD8^+$ T cell-mediated antitumor immunity (graphical summary in online supplemental file 1).

IL-10 was initially characterized as an immunosuppressive cytokine.[12] However, emerging evidence suggests that IL-10 plays a crucial role in enhancing antitumor immunity by promoting cytotoxic function of $CD8^+$ T cells, ultimately leading to improved survival outcomes.[15–17] Preclinical models and clinical trials using recombinant IL-10 have further demonstrated its therapeutic efficacy in primary tumor settings.[30 31] Mechanistically, IL-10 facilitates $CD8^+$ T-cell infiltration into tumor tissues, stimulates the production of IFN-γ and granzyme B of $CD8^+$ T cell, supports the development of effective memory T-cell responses, and revitalizes exhausted $CD8^+$ T cells within the tumor microenvironment.[15 19 32 33] Additionally, IL-10 reprograms $CD8^+$ T-cell metabolism toward oxidative phosphorylation, enhancing mitochondrial

respiratory capacity. This metabolic shift promotes the expansion and effector function of terminally exhausted CD8+ TILs.[33–35] Moreover, IL-10 directly induces the phosphorylation of STAT1 and STAT3 in CD8+ T cells, thereby enhancing their survival and proliferation, as observed in patients with gastric cancer.[36] In our study, we found that liver-directed delivery of AAV-IL-10 effectively inhibited orthotopic HCC tumor growth. This therapeutic effect was associated with the expansion of CD8+ Trm-like cells and the augmentation of effector functions in exhausted CD8+ TILs.

T-cell exhaustion arises from chronic tumor antigen exposure and is characterized by progressive differentiation into progenitor and terminally exhausted CD8+ T-cell states with distinct functional properties.[37 38] Exhausted CD8+ T cells can be classified into progenitor and terminally exhausted subsets. These subsets exhibit distinct functional properties: progenitor exhausted T cells are stem-like and can differentiate into terminally exhausted T cells. Terminally exhausted CD8+ T cells produce higher levels of effector molecules, such as IFN-γ and granzyme B, but have limited proliferative capacity and polyfunctionality compared with their progenitor counterparts.[37 38] Antigen-specific peptide stimulation selectively activates tumor-specific CD8+ T cells, whereas PMA/ionomycin induces antigen-independent activation and enables functional assessment of both tumor-specific and bystander CD8+ T cells. Accordingly, we combined H-2Kb-restricted $OVA_{257–264}$ tetramer labeling with PMA/ionomycin stimulation to evaluate exhaustion status and effector potential within intratumoral CD8+ T-cell populations. Using this approach, we found that AAV-IL-10 did not alter the relative proportions of progenitor and terminally exhausted OVA-specific CD8+ TILs but significantly enhanced effector molecule expression in terminally exhausted CD8+ TILs. In addition, AAV-IL-10 reduced the frequency of progenitor exhausted bystander CD8+ TILs, suggesting a broader impact on intratumoral CD8+ T-cell exhaustion dynamics. These findings are consistent with prior studies demonstrating IL-10–Fc fusion protein mediated functional enhancement of exhausted CD8+ T cells in a subcutaneous melanoma model[33] and support our liver-directed IL-10 delivery reinvigorates exhausted CD8+ T cells without reversing their differentiation state.

Trm cells are non-recirculating immune cells that permanently reside in peripheral tissues such as the skin, lungs, gut, female reproductive tract, and liver, where they serve as a first line of defense against local infections and tumors.[39–42] Trm cells are typically identified by the co-expression of memory markers together with CD69 and/or CD103. CD69, which also acts as an early activation marker, suppresses sphingosine-1-phosphate receptor-1 signaling to promote tissue retention.[43] CD103 serves as another canonical Trm marker; however, hepatic Trm cells frequently downregulate CD103 expression while maintaining other residency-associated markers.[40] Functionally, Trm cells combine features of both central memory and effector T cells, expressing molecules that support homeostatic survival and proliferation (eg, Ki-67, Bcl-2) alongside effector mediators such as IFN-γ, TNF-α, granzyme B, CD107a, and various co-inhibitory receptors.[40 41 44] Cells with a Trm-like phenotype have been identified across multiple human malignancies, including HCC.[45–49] Importantly, the presence of Trm-like CD8+ T cells within TILs has been correlated with improved patient outcomes, often representing a stronger prognostic indicator than total TIL abundance.[42 46–49] Collectively, these findings suggest that CD8+ Trm cells play a pivotal role in controlling HCC tumor progression.

In our study, liver-directed AAV-IL-10 treatment markedly increased the proportion of CD8+ TILs exhibiting a Trm-like phenotype within liver tumors, while such cells were absent from draining LNs. Notably, these IL-10-induced Trm-like CD8+ T cells persisted within the liver even after tumor regression, suggesting a potential role in long-term immune surveillance and protection against recurrence. Furthermore, our data indicate that the generation and maintenance of CD8+ Trm-like cells occur independently of lymph node-mediated priming. The comparable frequencies of OVA-specific Trm-like CD8+ T cells in FTY720-treated and control mice demonstrate that blockade of lymphocyte egress from LNs does not impair their accumulation in the liver. This finding supports a model in which CD8+ Trm-like cells can be primed or sustained locally within the hepatic microenvironment. Consistent with this interpretation, recent work has shown that intrahepatic CD8+ T-cell priming can occur via antigen presentation by Kupffer cells, facilitated by CD4+ T-cell help.[50] Our results align with and extend these observations, suggesting that IL-10-mediated modulation of the hepatic immune milieu may further promote the differentiation, retention, and longevity of liver-resident CD8+ Trm-like cells, thereby contributing to localized and durable antitumor immunity in HCC.

Recombinant IL-10 protein has a short half-life, necessitating frequent administration to sustain therapeutic levels.[22] In this study, we employed AAV-DJ, a recombinant adeno-associated virus derived from a hybrid capsid library of eight wild-type AAV serotypes. AAV-DJ combines capsid features that confer broad tissue transduction efficiency with a pronounced preference for hepatocytes, resulting in superior gene delivery to the liver compared with other serotypes.[51] AAV-IL-10 demonstrated superior transduction efficiency in the liver, as shown in figure 1. Notably, serum IL-10 levels remained relatively low (<5 ng/mL), which is substantially lower than those observed in previous studies using recombinant IL-10 protein, where peak serum levels reached approximately 100 µg/mL.[34] Additionally, our findings, along with previous reports, confirm that IL-10 expression is sustained for at least 10 weeks following AAV-IL-10 administration.[21]

Despite effective liver transduction, AAV-IL-10 treatment did not inhibit the growth of distant subcutaneous tumors, likely reflecting insufficient IL-10 bioavailability at those sites. Interestingly, both AAV-mock-treated and AAV-IL-10-treated subcutaneous tumors began to regress

around day 11 post-implantation, a phenomenon also observed in untreated mice (data not shown). We speculate that this spontaneous regression results from the inability of Hep55.1c cells to establish a supportive microenvironment within subcutaneous tissue, which lacks the growth-promoting and immunoregulatory factors present in the liver. Together, these findings highlight the potential of AAV-IL-10 as a liver-directed therapeutic approach, enabling sustained local IL-10 expression within the hepatic tumor microenvironment while minimizing systemic exposure.

Taken together, our study demonstrates that liver-directed IL-10 delivery enhances cytotoxic $CD8^+$ T-cell responses and augments the effector functions of $CD8^+$ tumor-infiltrating lymphocytes, leading to effective suppression of HCC growth. Importantly, AAV-mediated IL-10 delivery provides a reliable and long-lasting therapeutic strategy, enabling sustained local IL-10 expression and prolonged antitumor efficacy within the liver. These findings highlight a novel approach to overcoming hepatic immune suppression and enhancing liver-specific antitumor immunity in HCC. Nevertheless, the interpretation of our $CD8^+$ T-cell depletion experiments is limited by the small group size resulting from early humane endpoints, and these data should therefore be regarded as supportive rather than definitive evidence for $CD8^+$ T cell-dependent antitumor effects of AAV-IL-10. In addition, although our findings were validated in both orthotopic and intrahepatic metastatic liver tumor models, this study remains primarily based on murine systems; future studies employing additional in vivo models and human-relevant platforms, such as patient-derived organoids or ex vivo immune-tumor co-cultures, will be required to further establish the translational relevance of liver-directed AAV-IL-10 therapy.

Acknowledgements The authors would like to thank the 3rd Laboratory and the 7th Laboratory at the Department of Medical Research, National Taiwan University Hospital, for their technical support. We also acknowledged the AAV Core Facility of Academia Sinica in generating recombinant AAV (Grant AS-CFII112-204). We gratefully acknowledge the NIH Tetramer Core Facility (Emory University) for providing the H-$2K^b$ SIINFEKL tetramers used in this study.

Contributors Y-HC and C-IL designed the studies. C-IL, Y-WC, M-SY, Y-WW, and Y-HW conducted the experiments, analyzed data, and prepared data displays. Y-HC supervised the study and provided technical and conceptual guidance. Y-HC and C-IL wrote the manuscript with input from Y-WC, M-SY, Y-WW, and Y-HW. All authors discussed the results and approved the final version of the manuscript. Y-HC is the guarantor.

Funding This research was supported by the Ministry of Science and Technology, Taiwan (MOST 111-2320-B-002-060-MY3). The funders had no role in the design of the study; collection, analysis, or interpretation of data; or in writing the manuscript.

Competing interests None declared.

Patient consent for publication Not applicable.

Ethics approval Not applicable.

Provenance and peer review Not commissioned; externally peer reviewed.

Data availability statement Data are available upon reasonable request.

ORCID iD

Ya-Hui Chuang https://orcid.org/0000-0003-0857-0035

REFERENCES

1 Ringelhan M, Pfister D, O'Connor T, *et al*. The immunology of hepatocellular carcinoma. *Nat Immunol* 2018;19:222–32.
2 Kawashima K, Andreata F, Beccaria CG, *et al*. Priming and Maintenance of Adaptive Immunity in the Liver. *Annu Rev Immunol* 2024;42:375–99.
3 Hou J, Zhang H, Sun B, *et al*. The immunobiology of hepatocellular carcinoma in humans and mice: Basic concepts and therapeutic implications. *J Hepatol* 2020;72:167–82.
4 Flecken T, Schmidt N, Hild S, *et al*. Immunodominance and functional alterations of tumor-associated antigen-specific CD8+ T-cell responses in hepatocellular carcinoma. *Hepatology* 2014;59:1415–26.
5 Lu L, Jiang J, Zhan M, *et al*. Targeting Tumor-Associated Antigens in Hepatocellular Carcinoma for Immunotherapy: Past Pitfalls and Future Strategies. *Hepatology* 2021;73:821–32.
6 Guidotti LG, Inverso D, Sironi L, *et al*. Immunosurveillance of the liver by intravascular effector CD8(+) T cells. *Cell* 2015;161:486–500.
7 McVey JC, Green BL, Ruf B, *et al*. NAFLD indirectly impairs antigen-specific $CD8^+$ T cell immunity against liver cancer in mice. *iScience* 2022;25:103847.
8 Wada Y, Nakashima O, Kutami R, *et al*. Clinicopathological study on hepatocellular carcinoma with lymphocytic infiltration. *Hepatology* 1998;27:407–14.
9 Zheng C, Zheng L, Yoo J-K, *et al*. Landscape of Infiltrating T Cells in Liver Cancer Revealed by Single-Cell Sequencing. *Cell* 2017;169:1342–56.
10 Ma J, Zheng B, Goswami S, *et al*. PD1Hi CD8+ T cells correlate with exhausted signature and poor clinical outcome in hepatocellular carcinoma. *J Immunotherapy Cancer* 2019;7:331.
11 Wang X, He Q, Shen H, *et al*. TOX promotes the exhaustion of antitumor $CD8^+$ T cells by preventing PD1 degradation in hepatocellular carcinoma. *J Hepatol* 2019;71:731–41.
12 Ouyang W, Rutz S, Crellin NK, *et al*. Regulation and functions of the IL-10 family of cytokines in inflammation and disease. *Annu Rev Immunol* 2011;29:71–109.
13 Murai M, Turovskaya O, Kim G, *et al*. Interleukin 10 acts on regulatory T cells to maintain expression of the transcription factor Foxp3 and suppressive function in mice with colitis. *Nat Immunol* 2009;10:1178–84.
14 Giovarelli M, Musiani P, Modesti A, *et al*. Local release of IL-10 by transfected mouse mammary adenocarcinoma cells does not suppress but enhances antitumor reaction and elicits a strong cytotoxic lymphocyte and antibody-dependent immune memory. *J Immunol* 1995;155:3112–23.
15 Mumm JB, Emmerich J, Zhang X, *et al*. IL-10 elicits IFNγ-dependent tumor immune surveillance. *Cancer Cell* 2011;20:781–96.
16 Oft M. Immune regulation and cytotoxic T cell activation of IL-10 agonists - Preclinical and clinical experience. *Semin Immunol* 2019;44:101325.
17 Qiao J, Liu Z, Dong C, *et al*. Targeting Tumors with IL-10 Prevents Dendritic Cell-Mediated $CD8^+$ T Cell Apoptosis. *Cancer Cell* 2019;35:901–15.
18 Berman RM, Suzuki T, Tahara H, *et al*. Systemic administration of cellular IL-10 induces an effective, specific, and long-lived immune response against established tumors in mice. *J Immunol* 1996;157:231–8.
19 Naing A, Infante JR, Papadopoulos KP, *et al*. PEGylated IL-10 (Pegilodecakin) Induces Systemic Immune Activation, $CD8^+$ T Cell Invigoration and Polyclonal T Cell Expansion in Cancer Patients. *Cancer Cell* 2018;34:775–91.

20 Naing A, Papadopoulos KP, Autio KA, *et al*. Safety, Antitumor Activity, and Immune Activation of Pegylated Recombinant Human Interleukin-10 (AM0010) in Patients With Advanced Solid Tumors. *J Clin Oncol* 2016;34:3562–9.
21 Hsueh Y-H, Chen H-W, Syu B-J, *et al*. Endogenous IL-10 maintains immune tolerance but IL-10 gene transfer exacerbates autoimmune cholangitis. *J Autoimmun* 2018;95:159–70.
22 Huhn RD, Radwanski E, Gallo J, *et al*. Pharmacodynamics of subcutaneous recombinant human interleukin-10 in healthy volunteers. *Clin Pharmacol Ther* 1997;62:171–80.
23 Mingozzi F, High KA. Immune responses to AAV vectors: overcoming barriers to successful gene therapy. *Blood* 2013;122:23–36.
24 Ozelo MC, Mahlangu J, Pasi KJ, *et al*. Valoctocogene Roxaparvovec Gene Therapy for Hemophilia A. *N Engl J Med* 2022;386:1013–25.
25 Brown ZJ, Heinrich B, Greten TF. Mouse models of hepatocellular carcinoma: an overview and highlights for immunotherapy research. *Nat Rev Gastroenterol Hepatol* 2018;15:536–54.
26 Barbier L, Tay SS, McGuffog C, *et al*. Two lymph nodes draining the mouse liver are the preferential site of DC migration and T cell activation. *J Hepatol* 2012;57:352–8.
27 Wherry EJ, Kurachi M. Molecular and cellular insights into T cell exhaustion. *Nat Rev Immunol* 2015;15:486–99.
28 Franco F, Jaccard A, Romero P, *et al*. Metabolic and epigenetic regulation of T-cell exhaustion. *Nat Metab* 2020;2:1001–12.
29 Brinkmann V, Cyster JG, Hla T. FTY720: sphingosine 1-phosphate receptor-1 in the control of lymphocyte egress and endothelial barrier function. *Am J Transplant* 2004;4:1019–25.
30 Naing A, Wong DJ, Infante JR, *et al*. Pegilodecakin combined with pembrolizumab or nivolumab for patients with advanced solid tumours (IVY): a multicentre, multicohort, open-label, phase 1b trial. *Lancet Oncol* 2019;20:1544–55.
31 Spigel D, Jotte R, Nemunaitis J, *et al*. Randomized Phase 2 Studies of Checkpoint Inhibitors Alone or in Combination With Pegilodecakin in Patients With Metastatic NSCLC (CYPRESS 1 and CYPRESS 2). *J Thorac Oncol* 2021;16:327–33.
32 Emmerich J, Mumm JB, Chan IH, *et al*. IL-10 directly activates and expands tumor-resident CD8(+) T cells without de novo infiltration from secondary lymphoid organs. *Cancer Res* 2012;72:3570–81.
33 Guo Y, Xie YQ, Gao M, *et al*. Metabolic reprogramming of terminally exhausted CD8+ T cells by IL-10 enhances anti-tumor immunity. *Nat Immunol* 2021;22:746–56.
34 Chang Y-W, Hsiao H-W, Chen J-P, *et al*. A CSF-1R-blocking antibody/IL-10 fusion protein increases anti-tumor immunity by effectuating tumor-resident CD8$^+$ T cells. *Cell Rep Med* 2023;4:101154.
35 Zhao Y, Chen J, Andreatta M, *et al*. IL-10-expressing CAR T cells resist dysfunction and mediate durable clearance of solid tumors and metastases. *Nat Biotechnol* 2024;42:1693–704.
36 Xi J, Xu M, Song Z, *et al*. Stimulatory role of interleukin 10 in CD8$^+$ T cells through STATs in gastric cancer. *Tumour Biol* 2017;39:1010428317706209.
37 Miller BC, Sen DR, Al Abosy R, *et al*. Subsets of exhausted CD8+ T cells differentially mediate tumor control and respond to checkpoint blockade. *Nat Immunol* 2019;20:326–36.
38 Siddiqui I, Schaeuble K, Chennupati V, *et al*. Intratumoral Tcf1+PD-1+CD8+ T Cells with Stem-like Properties Promote Tumor Control in Response to Vaccination and Checkpoint Blockade Immunotherapy. *Immunity* 2019;50:195–211.
39 Tse S-W, Radtke AJ, Espinosa DA, *et al*. The chemokine receptor CXCR6 is required for the maintenance of liver memory CD8(+) T cells specific for infectious pathogens. *J Infect Dis* 2014;210:1508–16.
40 Fernandez-Ruiz D, Ng WY, Holz LE, *et al*. Liver-Resident Memory CD8$^+$ T Cells Form a Front-Line Defense against Malaria Liver-Stage Infection. *Immunity* 2016;45:889–902.
41 Schenkel JM, Masopust D. Tissue-resident memory T cells. *Immunity* 2014;41:886–97.
42 Park SL, Gebhardt T, Mackay LK. Tissue-Resident Memory T Cells in Cancer Immunosurveillance. *Trends Immunol* 2019;40:735–47.
43 Steinert EM, Schenkel JM, Fraser KA, *et al*. Quantifying Memory CD8 T Cells Reveals Regionalization of Immunosurveillance. *Cell* 2015;161:737–49.
44 Steinbach K, Vincenti I, Kreutzfeldt M, *et al*. Brain-resident memory T cells represent an autonomous cytotoxic barrier to viral infection. *J Exp Med* 2016;213:1571–87.
45 Lim CJ, Lee YH, Pan L, *et al*. Multidimensional analyses reveal distinct immune microenvironment in hepatitis B virus-related hepatocellular carcinoma. *Gut* 2019;68:916–27.
46 Edwards J, Wilmott JS, Madore J, *et al*. CD103$^+$ Tumor-Resident CD8$^+$ T Cells Are Associated with Improved Survival in Immunotherapy-Naïve Melanoma Patients and Expand Significantly During Anti-PD-1 Treatment. *Clin Cancer Res* 2018;24:3036–45.
47 Savas P, Virassamy B, Ye C, *et al*. Single-cell profiling of breast cancer T cells reveals a tissue-resident memory subset associated with improved prognosis. *Nat Med* 2018;24:986–93.
48 Djenidi F, Adam J, Goubar A, *et al*. CD8+CD103+ tumor-infiltrating lymphocytes are tumor-specific tissue-resident memory T cells and a prognostic factor for survival in lung cancer patients. *J Immunol* 2015;194:3475–86.
49 Gebhardt T, Park SL, Parish IA. Stem-like exhausted and memory CD8+ T cells in cancer. *Nat Rev Cancer* 2023;23:780–98.
50 Venzin V, Beccaria CG, Perucchini C, *et al*. CD4+ T cells license Kupffer cells to reverse CD8+ T cell dysfunction induced by hepatocellular priming. *Nat Immunol* 2025;26:1352–66.
51 Grimm D, Lee JS, Wang L, *et al*. In vitro and in vivo gene therapy vector evolution via multispecies interbreeding and retargeting of adeno-associated viruses. *J Virol* 2008;82:5887–911.